Optics Communications 285 (2012) 4235–4240

Contents lists available at SciVerse ScienceDirect

Optics Communications

journal homepage: www.elsevier.com/locate/optcom

All-around holographic three-dimensional light field display

Dongdong Teng, Lilin Liu, Zixin Wang, Bixiong Sun, Biao Wang*

School of Physics and Engineering, Sun Yat-Sen University, 135 Xingang West Road, Haizhu District, Guangzhou, Guangdong Province 510275, PR China

ARTICLE INFO

Article history:
Received 31 January 2012
Received in revised form
13 June 2012
Accepted 16 June 2012
Available online 2 July 2012

Keywords:
CGH
3D
Light field display
Mirror-image

ABSTRACT

Technology for all-around holographic three-dimensional (3D) light field display is proposed in this paper. A plane mirror keeps rotating around the optical axis. At each angular position, the mirror-image's Fourier CGH of the target object is projected onto the mirror. The reflected CGH contributes a specific viewing angle range to the target object. Linking up all viewing angle ranges in the horizontal plane, all-around display can be realized via the "afterimage" effect. An all-around holographic 3D light field display is implemented experimentally here with a 60 Hz SLM by introducing an observer tracking unit in the proposed display system.

1. Introduction

Reconstructing the wave front emitted from a three-dimensional (3D) object, a computer generated hologram (CGH) was thought as an ideal technique which provides a natural spatial effect. However, both the viewing angle and size of the hologram depend on the space-bandwidth characteristics of the spatial light modulator (SLM). An extremely high-resolution SLM is required to produce practical 3D light fields. Present SLMs usually have a resolution of 100–200 lines/mm and $10^3 \times 10^3$ pixels. Hence, the viewing angle of a 3D light field produced through this technique is limited to several degrees and cannot be observed by both eyes.

A lot of alternative methods were tried. Mishina et al. proposed a time multiplexing method that uses the high-order light diffraction to double the viewing angle [1]. In the work of Stanley et al. [2], de-magnified images generated by a high-speed SLM were tiled onto an optically addressed SLM in a time-sequential manner to produce a 3D light field, which was called "active tiling technique". Techniques by using multiple SLMs were developed by several researchers [3]. In addition, the research group of Takaki reported a resolution redistribution system [4] and a horizontally scanning system [5]. Although the viewing angle becomes wider with these methods, they could not realize all-around holographic 3D light field display.

Jones et al. reported an all-around light field display system by projecting over 5000 two-dimensional images onto a spinning mirror covered by a complicated holographic diffuser [6]. But as a binocular parallax technology, the visual accommodation remains to be a problem and the resolution of the light field is limited by the degree of separation between adjacent images.

In this article, instead of 2D images, we project 3D CGHs with small viewing angle onto a spinning planar mirror. The reconstructed all-around 3D light field is with all the monocular and binocular visual cues and suitable for people with only one eye also.

2. Fourier CGH

Fourier CGH is adopted in this article, that is, the reconstructed light field is the Fourier transformation of the two-dimensional message modulated by the SLM. If the pixel pitch of the SLM is denoted by p, the modulation plane can be expressed as $M_x p \times M_y p$, where M_x and M_y are the resolutions along x and y directions, respectively. Along x and y directions, the viewing angle ranges of all the points on the Fourier CGH are equivalent and determined by

$$\theta_x = 2arctg(M_x p/2f) \quad (1-1)$$

$$\theta_y = 2arctg(M_y p/2f) \quad (1,-2)$$

and the maximum size of the Fourier CGH is given by

$$D_x = D_y = \lambda f/p \quad (1-3)$$

where f is the focal length of the Fourier transform lens and λ is the wavelength of the normal incident light.

3. Enlargement of the viewing angle

The display consists of a SLM, a Fourier transform lens and a plane mirror which is called directional-reflection mirror in this

* Corresponding author. Tel.: +86 1343 397 5953.
E-mail addresses: tengdd@mail.sysu.edu.cn (D. Teng), liullin@mail.sysu.edu.cn (L. Liu).

0030-4018/$ - see front matter © 2012 Elsevier B.V. All rights reserved.
http://dx.doi.org/10.1016/j.optcom.2012.06.037

paper. Its schematic optical diagram is shown in Fig. 1. The optical axis is coincident with the z-axis and the SLM is located at the front focal plane of the Fourier transform lens. The directional-reflection mirror, which is set as $\alpha=45^\circ$ with respect to the z-axis, rotates around the z-axis and intersects with the back focal plane at point O. The point O is used as the coordinate origin.

A series of Fourier CGHs generated by the SLM are projected onto the rotating directional-reflection mirror in a time-sequential manner and then reflected out into surrounding viewing areas. The start angular position of the rotating directional-reflection mirror, position “0”, is defined as the position in which the mirror surface is parallel to the y-axis and the reflective light propagates along the negative direction of the x-axis, as shown in Fig. 1. The “display space” is the overlapping space of the zeroth-order diffraction light, as shown in Fig. 1. For simplicity, we assume a solid-line triangle in the x–z plane to represent the target object, which is placed in the “display space” virtually. With the directional-reflection mirror frozen at a particular angular position, “position n”, the mirror-image of the target object with respect to the mirror at this position is defined as the elementary mirror-image “n” (*EMI* “n”).

When the directional-reflection mirror rotates to the position “0”, the Fourier CGH of *EMI* “0” is generated by the SLM and projected onto the mirror. *EMI* “0” is shown by a dashed-line triangle in Fig. 1. Any point on the *EMI* “0”, for example a', is reflected by the mirror and its reflection image on the virtual target image – point a – is the luminous spot that the observer can see. The viewing angle of the point a is denoted by $\theta_{0\parallel}$ and $\theta_{0\perp}$, where the subscript “0” means the position of the mirror. The subscript “$\parallel$” denotes a horizontal viewing angle in the plane $S_\perp$ which is perpendicular to the z-axis and passes through the point a. The subscript “$\perp$” represents the vertical viewing angle in the plane containing the z-axis and the point a.

Then, rotating the directional-reflection mirror to the next angular position “1”, the Fourier CGH of EMI “1” is projected onto the mirror. There must exist a point “a” on the EMI “1”, which has a mirror image relationship with the point a. Hence, the point a gets a new viewing angle of $\theta_{1\parallel}$ and $\theta_{1\perp}$. If the horizontal viewing angle $\theta_{0\parallel}$ and $\theta_{1\parallel}$ are designed to be adjacent, the object point a becomes observable in a wider angle range of $\theta_{0\parallel}+\theta_{1\parallel}$, as shown in Fig. 2.

As has been stated in Section 2, Fourier CGHs have a universal characteristic, that is, all points on the Fourier CGH of an *EMI* have identical diffraction angles. These points are reflected by the directional-reflection mirror and the reflected diffraction angles remain being identical. The reflected points are in fact the luminous points on the virtual target object that the observer can see. Therefore, all points on the observed target object have the same viewing angle range as the point a.

For a target object being constituted by many points, there exist some observation locations where the observer cannot see the entire reconstructed object simultaneously. Schematically, three points b, c and d are used to represent a target object in the x–y plane, as shown in Fig. 3. When the mirror is frozen at position “0”, the reconstructed *EMI* “0” is reflected by the mirror. All three points could be seen by the eye at the location 1. However, the point d becomes invisible when the eye moves to the location 2. At this location, the point d becomes visible only when the mirror rotates to position “1”. The reconstructed *EMI* “1” is reflected by the mirror in this case.

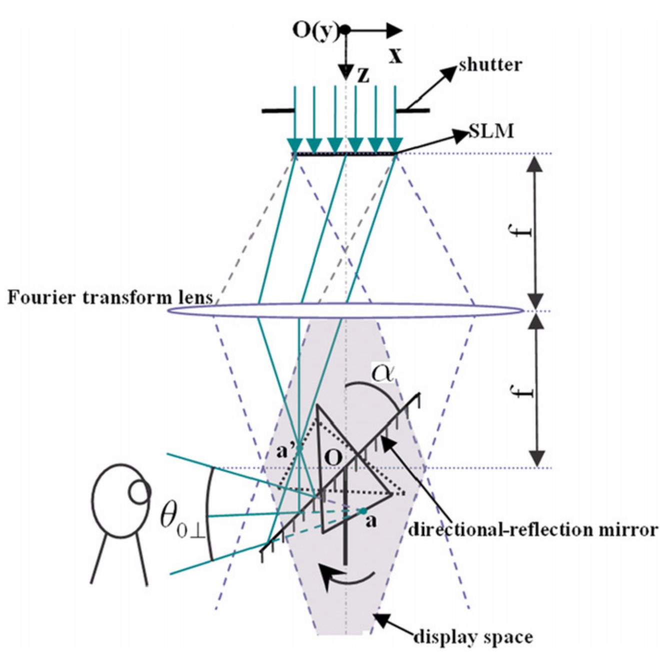

Fig. 1. Schematic optical diagram of the holographic 3D light field display system.

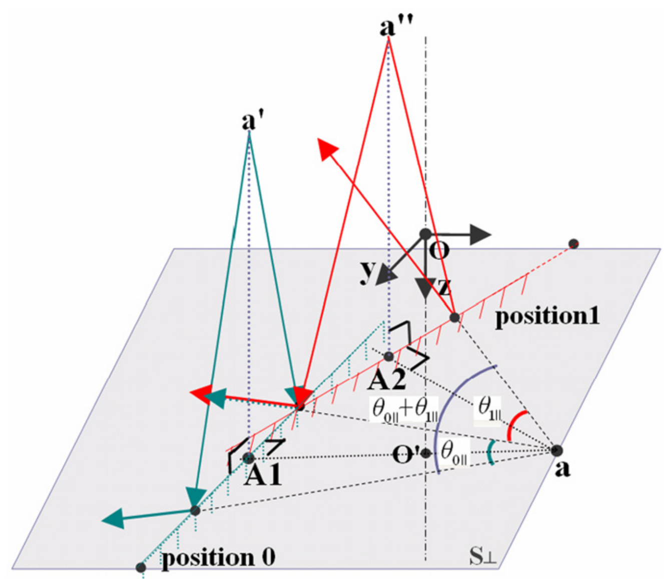

Fig. 2. Schematic optical diagram showing the idea of enlarging the viewing angle.

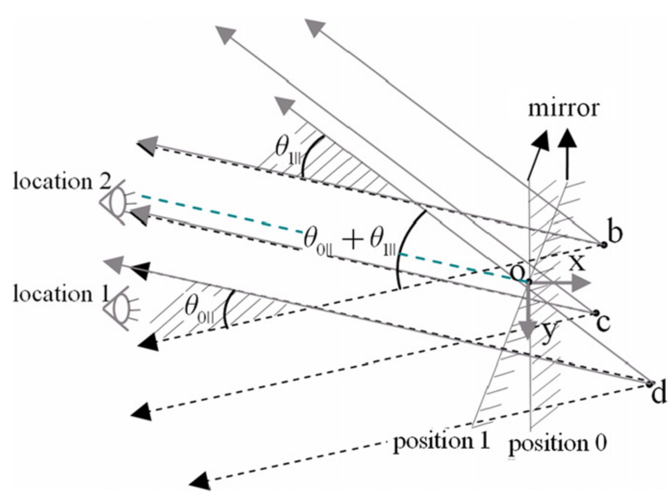

Fig. 3. A schematic optical diagram showing the visible/invisible points for the eye at different positions.

If both the frame rate of the SLM and the rotating speed of the directional-reflection mirror are high enough, the receptors in the human eye will have a temporal persistence due to mental processing delay, that is, the so-called "afterimage" effect. Therefore, human eye will fuse the light reflected from the two EMIs and receive the entire target object in a larger viewing angular region of $\theta = \theta_{0\parallel} + \theta_{1\parallel}$, as shown in Fig. 3.

In the same way, rotating the directional-reflection mirror to different angular positions, CGHs of the corresponding EMIs are projected synchronously. Hence horizontal viewing angle ranges along different viewing directions can be obtained. Linking up all n adjacent horizontal viewing angle ranges and using a SLM with high frame rate, the target object with a viewing angle range of $\theta = \theta_{0\parallel} + \cdots + \theta_{n\parallel}$ can be obtained due to the "afterimage" effect.

4. Determination of the angular positions

To implement a 3D display with the developed technology, all angular positions of the directional-reflection mirror must be determined.

The coordinate system in Fig. 4 has the same definition as that in Fig. 1. Assuming that a point P' of the CGH is on the z-axis, the distance between P' and the coordinate origin O is d. The object point corresponding to P' is denoted by P_m for the mirror being at the position "m", as shown in Fig. 4. The light field diffracted from point P' is confined within a rectangular region $(M_x p/f)d \times (M_y p/f)d$ in the x–y plane. Q_m and $Q_{m'}$ are the intersection points of the mirror surface with the sides of the rectangle. According to the geometrical relationship shown in Fig. 4, $\theta_{m\parallel}$, which denotes the horizontal viewing angle of point P_m, is equal to $\angle Q_m P' Q_{m'}$. All other points on the target object have similar geometrical relationship.

For the angular position of the mirror at the position "m", θ_m is the angle between the negative y-axis and the intersecting line of the mirror surface with the x–y plane. Following the geometrical relationship shown in Fig. 4, we obtain

$$\theta_{m\parallel} = 2arctan(\tan(0.5\theta_y)/\cos(\theta_m)). \quad (2)$$

Obviously, $\theta_{m\parallel}$ changes with the position of the directional-reflection mirror. For $m=0$, it can be seen that $\theta_{0\parallel} = \theta_y$. θ_y can be derived out through Eqs. (1)(2).

Basing on Eq. (2) and letting

$$\theta_{0\parallel}/2 + \theta_{1\parallel}/2 = \theta_1, \quad (3)$$

θ_1 and $\theta_{1\parallel}$can be obtained. And letting

$$\theta_{0\parallel}/2 + \theta_{1\parallel} + \theta_{2\parallel}/2 = \theta_2, \quad (4)$$

θ_2 and $\theta_{2\parallel}$ can be obtained. All the other angular positions in the 360° range, from θ_3 to θ_N, can be determined by the same method.

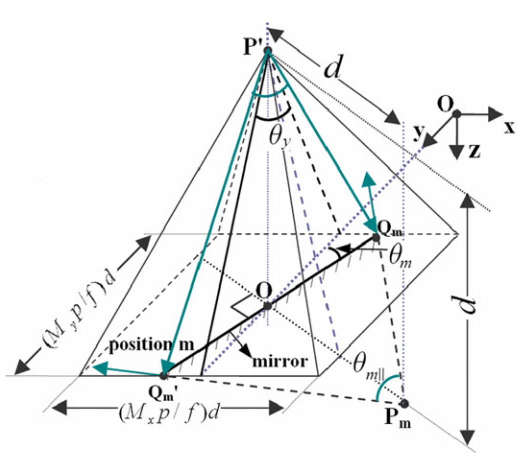

Fig. 4. Geometric diagrams showing the horizontal viewing angle with the mirror at position "m".

5. 360 degree all-around 3D light field display

Employing a high-speed SLM, the CGH of the nth EMI is projected onto the directional-reflection mirror when it rotates to the nth position. With all the N EMIs projected onto the rotating mirror time-sequentially and alternatively, a holographic 3D target object can be seen from all around just as if it is really there.

When the frame rate of the SLM is not high enough, the display of all the N EMIs will encounter the problem of obvious image flicker. An observer tracking unit can be introduced to solve this problem and realize an all-around display.

Range sensors are attached around the fixed base plate of the display system. These sensors can detect the position of the observer. As shown in Fig. 5, when the directional-reflection mirror

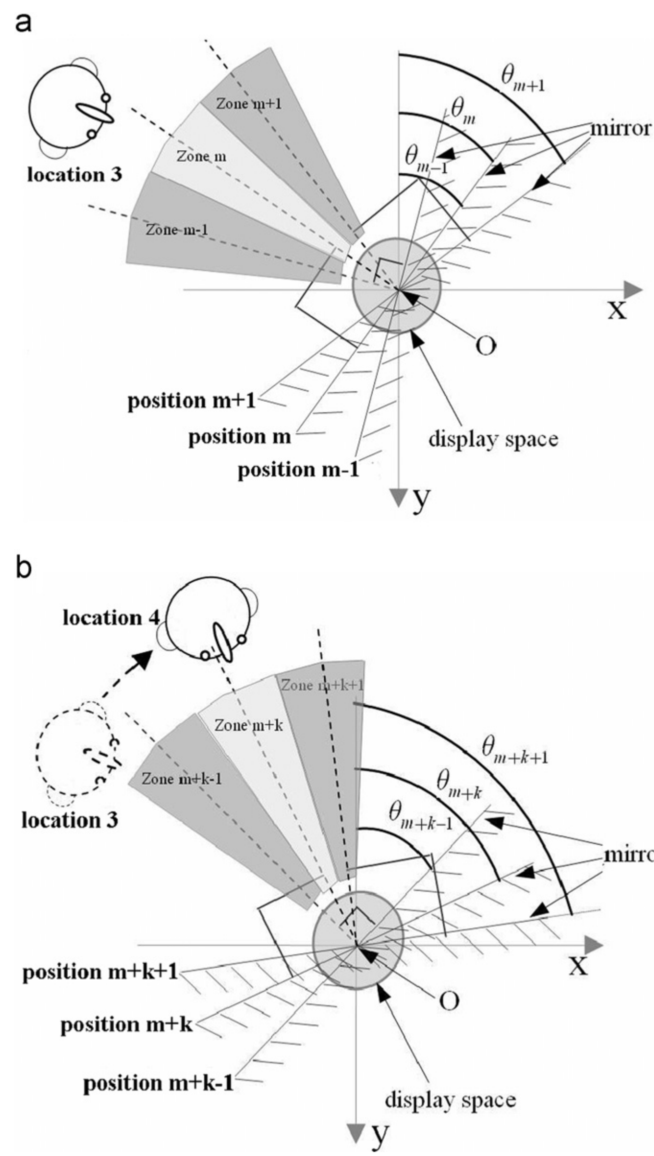

Fig. 5. Schematic optical diagrams showing the idea of directing right images to eyes of the moving observer by using only a few adjacent EMIs. (a) EMI "$m-1$", "m" and "$m+1$" being projected when the observer is close to Zone m; (b) EMI "$m+k-1$", "$m+k$" and "$m+k+1$" being projected when the observer is close to Zone $m+k$.

is located at the position “m”, we define the viewable region of the coordinate origin as Zone m.

When the observer stands at one location, the wavefront information outside the region occupied by the observer is wasted. Hence, only CGHs of a few neighbored EMIs are needed for fusing to a feasible 3D holographic display. The number of the neighbored EMIs, M, should be set enough to ensure that the distribution region of the displayed wavefront information covers both eyes of the observer.

Assuming $M=3$, CGHs of EMI “$m-1$”, “m” and “$m+1$” are projected onto the mirror and a binocular visible 3D light field is directed to the observer at a location being close to Zone m. Then, when the observer moves to Zone $m+k$, CGHs projected by the SLM change to those of EMI “$m+k-1$”, “$m+k$” and “$m+k+1$”. As shown in Fig. 5, the observer can see different views of the target object when he moves to a different location as if the 3D object really exists in the display space.

Hence, by introducing a tracing unit to detect the observer's location, the moving observer can receive the right view of the target object all the time through a non-high-speed SLM.

6. Experiment implementation

A display system is set up to implement the idea described above, as shown in Fig. 6, which consists of an electric shutter, a laser with a wavelength 532 nm, a reflective SLM, six sensors around the base plate every 60°, a directional-reflection mirror on the rotating device and some optical elements. HEO-1080 SLM from Holoeye Photonics AG with a frame rate of 60 Hz is used here, which is a pure phase modulator with a resolution of $1920\times1080\, M_x\times M_y$ and pixel size of $8\times8\ \mu m^2$. The inclination angle of the SLM, β, is set as 4° and the incident light can approximately be seen as normal incidence. The SLM and shutter are controlled by a computer. The focal length of the Fourier transform lens is 150 mm. The real photo of the experimental setup is shown in Fig.7.

Iteration algorithms are used for holographic encoding which features a loop of light propagation between adjacent object planes and the SLM plane [7,8]. As shown in Fig.8, an EMI is sliced into N object planes with equal interval, $\delta d=0.5\ mm$. P_1 is the nearest object plane and its distance to the Fourier transform lens is d. The SLM plane, P_{SLM}, is placed on the focal plane. The intensity distribution of the kth plane is denoted as $A(P_k)$. The maximum intensity value of $A(P_k)$ is 255 in an 8-bit bitmap file, but the minimum intensity value is set to be 3 according to Ref. [8]. The algorithm is described as follows:

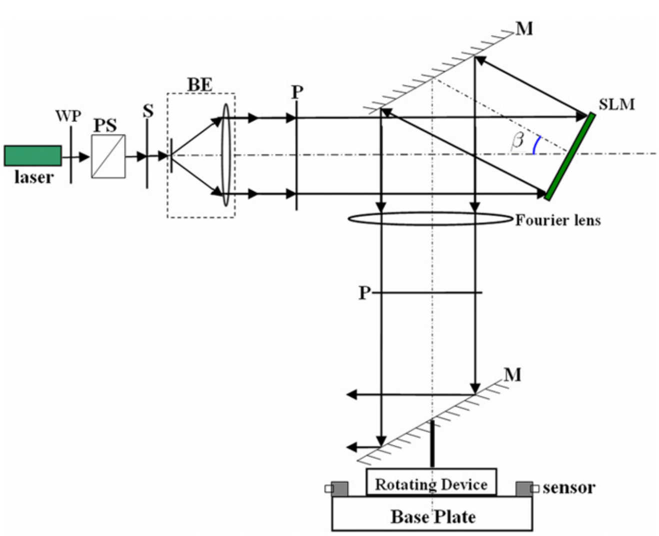

Fig. 6. Schematic drawing of the experimental setup. WP: ½ wave plate; PS: polarization splitter; S: shutter; BE: beam expander; P: polarizer; M: mirror.

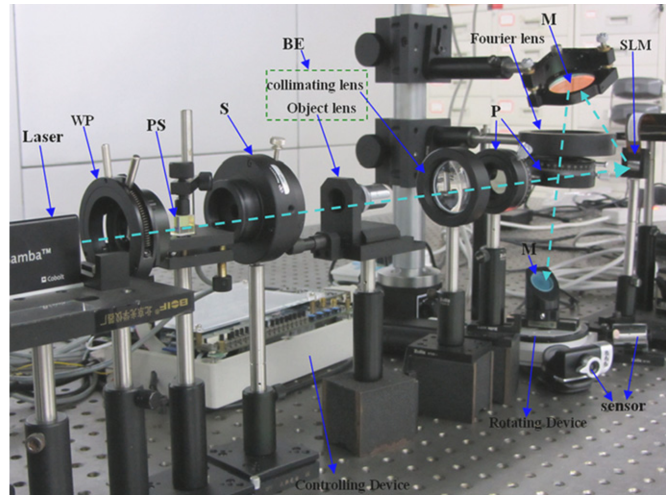

Fig. 7. Real photo of the experimental setup. Green arrows (dashed line) denote light propagations. Green arrows denote light propagations.WP: 1/2wave plate; PS: polarization splitter; S: shutter; BE: beam expander; P: polarizer; M: plane mirror. (For interpretation of the references to color in this figure legend, the reader is referred to the web version of this article.)

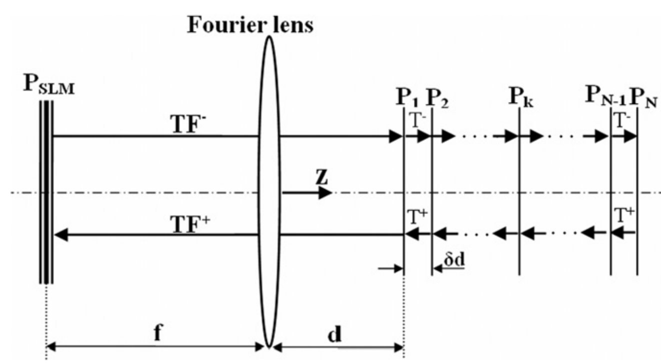

Fig. 8. The scheme of algorithm process.

1. A random-generated phase distribution is set as the original input phase of the P_{SLM}:U_{PSLM};
2. Propagation from P_{SLM} to $P_1(\mathrm{TF}^-)$:

$$\begin{aligned}U_{P1}(x_{P1},y_{P1})&=A(x_{P1},y_{P1})\exp[i\varphi(x_{P1},y_{P1})]\\&=F^{-1}i\lambda f\exp[-ik(1/2f)(1-d/f)(x_{PSLM}^2\\&\quad+y_{PSLM}^2)]U_{PSLM}(x_{PSLM},y_{PSLM});\end{aligned}$$

3. Amplitude adjustment in P_1:

$$U_{P1}(x_{P1},y_{P1})=A(P_1)\exp[i\varphi(x_{P1},y_{P1}))];$$

4. Propagation from P_1 to $P_2(\mathrm{T}^-)$:

$$\begin{aligned}U_{P2}(x_{P2},y_{P2})&=A(x_{P2},y_{P2})\exp(i\varphi(x_{P2},y_{P2}))\\&=F^{-1}\exp(-jk\delta d\sqrt{1-(\lambda f_x)^2-(\lambda f_y)^2})F[U_{P1}(x_{P1},y_{P1})]\end{aligned}$$

5. Amplitude adjustment in P_2:

$$U_{P2}(x_{P2},y_{P2})=A(P_2)\exp[i\varphi(x_{P2},y_{P2})];$$

6. Using the same method as step 4 and step 5 from P_2 to P_N, after $N-2$ operations, we obtain
$U_{PN}(x_{PN},y_{PN})=A(P_N)\exp[i\varphi(x_{PN},y_{PN})]$

7. Propagation from P_N to $P_{N-1}(\mathrm{T}^+)$:
$$\left(\begin{aligned} &U_{PN-1}(x_{PN-1},y_{PN-1})=A(x_{PN-1},y_{PN-1})\exp(i\varphi(x_{PN-1},y_{PN-1}))\\ &\quad=F^{-1}\exp(jk\delta d\sqrt{1-(\lambda f_x)^2-(\lambda f_y)^2})F[U_{P1}(x_{PN-1},y_{PN-1})]\end{aligned}\right)$$

8. Amplitude adjustment in P_{N-1}:
$U_{PN-1}(x_{PN-1},y_{PN-1})=A(P_{N-1})\exp[i\varphi(x_{PN-1},y_{PN-1})]$;

9. Using the same method as step 7 and step 8 from P_{N-1} to $P1$, after N$-$2 operations, we obtain
$U_{P1}(x_{P1},y_{P1})=A(P_1)\exp[i\varphi(x_{P1},y_{P1})]$

10. Propagation from P_1 to P_{SLM} (TF^+):
$$\begin{aligned} &U_{PSLM}(x_{PSLM},y_{PSLM})=A(x_{PSLM},y_{PSLM})\exp[i\varphi(x_{PSLM},y_{PSLM}))]\\ &\quad=\exp[ik(1/2f)(1-d/f)(x_{PSLM}^2+y_{PSLM}^2)]FU_{P1}/i\lambda f\end{aligned}$$

11. Amplitude adjustment in P_{SLM}:
$U_{PSLM}(x_{PSLM},y_{PSLM})=\exp[i\varphi(x_{PSLM},y_{PSLM}))]$

12. Repeating step 2 to step 11 for 500 times, the obtained U_{PSLM} is taken as the final input phase of the SLM.

Here $k=2\pi/\lambda$. F denotes Fourier transform operator and F^{-1} denotes inverse Fourier transform operator.

In the experiment, $\theta_{m\parallel}$ is set slightly smaller than the value deduced from Eq. (2) . A number of 84 EMIs are needed to provide all the views of the target object in a 360° viewing angle range. To avoid obvious image flicker, the frame rate of each EMI is set as 20 Hz. Hence, three adjacent EMIs are fused to present the 3D target object to the observer. The minimum viewing angle range is about 10° when EMI "84", "0" and "1" are projected. The 3D target object with this viewing angle is visible to both eyes of the observer who is 300 mm away from the display system.

Using sensors to detect the observer's location, the corresponding three neighbored EMIs are determined. The directional-reflection mirror keeps rotating at 60 rps. During each rotating period of the mirror, the holographic phase code of a chosen EMI is loaded into the SLM and the electric shutter closes until the mirror rotates to the corresponding position. Three chosen EMIs are projected onto the mirror time-sequentially and alternately.

Fig. 8(a) shows the target 3D object, a teapot with a size of $9.75\times6.75\times7.85\ \mathrm{mm}^3$. For coding, the teapot is cut into a series of parallel planes with an equal plane distance of 0.2 mm.

A camera is put at location 2 in Fig. 3. Fig. 8(b) and (c) shows the captured partial objects when the directional-reflection mirror is frozen at position "0" and position "1", respectively. EMI "0" and "1" are projected onto the mirror accordingly. The bright spot in the picture correspond to the point O in Fig. 3, which is non-diffraction light reflected from the SLM. Superposing Fig. 8(b) and (c) digitally, an entire image of the object is obtained, as shown in Fig. 8(d). It can be seen that the bright spots of Fig. 8(b) and (c) overlap precisely.

When the 3D display system works, an entire 3D teapot is presented to the observer at any viewing location. Fig. 9 shows the captured images with the camera being at locations –50°, 30°, 140° and 250° around the display space. The locations are given as their angular displacements with respect to the negative x-axis in Fig. 5. The bright spot at point O is weakened by a filter (Fig. 10).

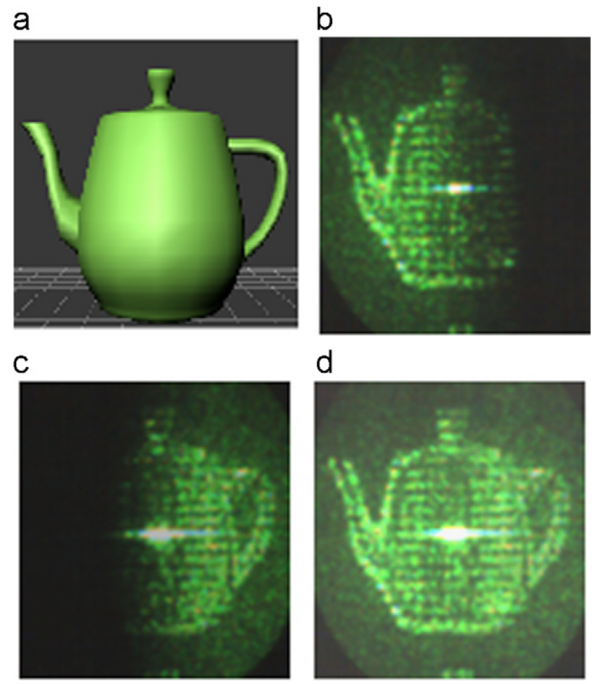

Fig. 9. (a) The target 3D image—a teapot. (b) The captured image at location 2 by a camera with EMI "0" being projected onto the mirror frozen at position "0". (c) The captured image at location 2 by a camera with EMI "1" being projected onto the mirror frozen at position "1". (d) The superposed graph of (b) and (c).

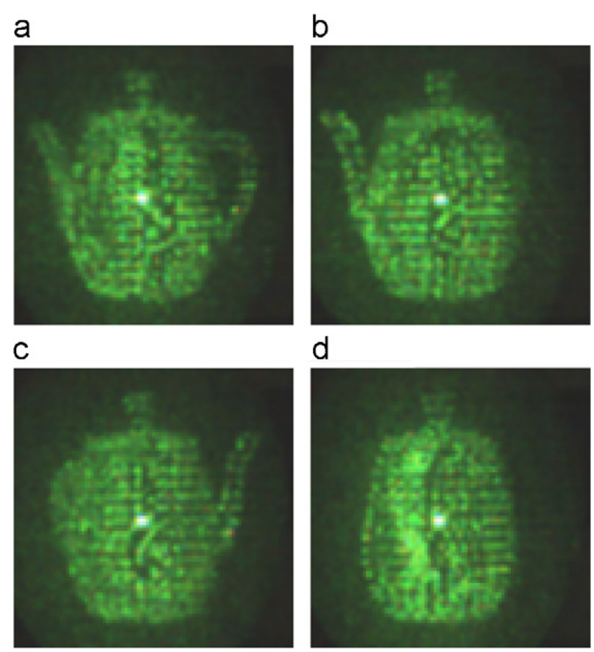

Fig. 10. Captured images when the display system works with the camera being at angular displacements of (a) $-50°$, (b) 30°, (c) 140° and (d) 250° with respect to the negative x-axis in Fig. 5.

7. Conclusion

A technique for all-around holographic 3D light field display is proposed in this paper. In the case that the frame rate of the SLM is not high enough, a 360° viewable area can still be implemented by introducing an observer tracking unit. Taking a teapot of $9.75 \times 6.75 \times 7.85$ mm^3 as the target object, an all-around holographic 3D display is realized by the display system with an observer tracking unit experimentally. The observer receives the right light field all time along when he moves around the system. The reconstructed 3D light field is with all the monocular and binocular visual cues.

Limited by performances of the used SLM (60 Hz) in the present work, the display system only accommodates one observer. For a SLM with higher frame rate, a multi-observer display system could be implemented by the proposed technology. On the other hand, as a matter of fact, some ferroelectric SLMs with frame rates of thousands of Hz have begun to appear in the market [9].

Acknowledgment

This paper was supported by the Natural Science Foundation of China under Grant no.10802101, the Reserve fund Natural Science Foundation of China under Grant nos. 11072271, 10972239, and 61007026 and personnel training of Sun Yat-Sen University under Grant no. 1132493.

References

[1] T. Mishina, F. Okano, I. Yuyama, Applied Optics 38 (1999) 3703.
[2] M. Stanley, R.W. Bannister, C.D. Cameron, S.D. Coomber, I.G. Gresswell, J.R. Hughes, V. Hui, P.O. Jackson, K.A. Milham, R.J. Miler, D.A. Payne, J. Quarrel, D.C. Scattergood, A.P. Smith, M.A.G. Smith, D.L. Tipton, P.H. Watson, P.J. Webber, C.W. Slinger, Proceedings of SPIE 5005 (2003) 247.
[3] F. Yaras, H. Kang, L. Onural, Optics Express 19 (2011) 9147.
[4] Y. Takaki, J. Nakamura, Optics Express 19 (2011) 14707.
[5] Y. Takaki, N. Okada, Applied Optics 48 (2009) 3255.
[6] A. Jones, I. McDowall, H. Yamada, M. Bolas, P. Debevec, ACM Transactions on Graphics 26 (2007) 40.1.
[7] M. Makowski, G. Mikula, M. Sypek, A. Kolodziejczyk, Optical Engineering 44 (2005) 125805.
[8] M. Makowski, M. Sypek, A. Kolodziejczyk, G. Mikula, J. Suszek, Optical Engineering 46 (2007) 045802.
[9] ⟨http://www.bnonlinear.com/products/xyslm/flc.pdf⟩.